Chapter 6

Bioorthogonal Labeling of *p*-AcPhe Incorporated in the Nicotinic Acetylcholine Receptor in *Xenopus* Oocytes

&

Western Blot Determination of the Subunit Stoichiometry of the Nicotinic Acetylcholine Receptor in *Xenopus* Oocytes

6.1 Introduction

Recent work has established new techniques to specifically label proteins *in vitro* and *in vivo* using genetically encoded sequences or small molecules with chemical functionalities unique from those found in living cells. These peptide sequences, unnatural sugar analogs, unnatural biotin moieties, and unnatural amino acids (UAAs) allow for specific labeling by a "bioorthogonal" small molecule reporter through enzymatic or chemical reaction (1). The tetracysteine motif has been utilized to selectively react with bisarsenical fluorescent dyes, such as FlAsH and ReAsH (2,3). A 15 amino acid sequence has been utilized to attach a biotin or an unnatural biotin that contains a ketone moiety to a protein using the *E. coli* biotin ligase (4,5). Unnatural sugar analogs with ketones, aldehydes, and azides have been incorporated *in vivo* using endogenous enzymes and labeled with biotin for purification or fluorophores for imaging (1,6–12). UAAs have been incorporated *in vivo* using endogenous aminoacyl tRNA-synthetases, mutant aminoacyl tRNA-synthetases, or an orthogonal tRNA/synthetase pair to incorporate ketones, aldehydes, diketones, azides, and alkynes and labeled with biotin and fluorophores (13–22).

The ketone functionality has been used extensively to label glycosylated proteins containing unnatural sugar analogs and proteins containing UAAs. The ketone is biorestricted in that it is bioorthogonal only on the cell surface because the interior of the cell contains acetylated proteins and keto/aldehydic metabolites (1). The ketone has been used extensively to label proteins *in vitro* that are purified or in crude cell lysates from *E. coli*, HEK 293T cells, and rat neurons (4,6,19,20). The ketone has also been used to label proteins on the cell surface of *E. coli*, jurkat cells, HL-60 cells, and HeLa cells

(4,10,11,13,20). In this research, we incorporated the UAA *p*-Acetyl-L-phenylalanine (*p*-AcPhe) into the α-subunit of the mouse muscle nicotinic acetylcholine receptor (nAChR) expressed in *Xenopus* oocytes and attempted to site-specifically label with biotin hydrazide and cyanine5.5 (Cy5.5) hydrazide.

Many membrane proteins form multimeric complexes, and the stoichiometry is precisely regulated by the insertion into the endoplasmic reticulum, folding transitions, post-translational modification, interactions with other subunits and/or chaperones, forming the final oligomeric complex (for many membrane proteins), subsequent transport to the golgi (where further oligomerization can take place), and export to the cell membrane (where further oligomerization can also occur) (23–29). To add further complexity, many ion channels are heteromeric and contain different subunits. For example, for the nAChRs there are ten α-subunits (α_1-α_{10}), four β-subunits (β_1-β_4), a γ-subunit, a δ-subunit, and an ε-subunit. These subunits can form homomeric channels ($5\alpha_7$) and heteromeric channels ($2\alpha_1$:β_1:γ:δ, α_1:β_1:γ:δ:ε, $2\alpha_3$:$3\beta_4$, $3\alpha_4$:$2\beta_2$, and $2\alpha_4$:$3\beta_2$) (30). For seventeen genes there is a possibility of 283,985 combinations, but most are not biologically relevant.

Determining subunit stoichiometry in ion channels can be complicated. Classically, macroscopic or single-channel electrophysiology recordings have been used to predict the subunit composition when analyzing inactivation or expressing wild-type and mutant channels with altered conductances (31–33). However, electrophysiology can't always accurately predict the subunit stoichiometry of ion channels. For example, cyclic nucleotide-gated (CNG) channels were thought to have a stoichiometry of 2CNGA1:2CNGA2 (34), but recent FRET experiments (35) and biochemical analysis

(36) have shown that the channels have a stoichiometry of 3CNGA1:CNGA2. Recent experiments have attached GFP to ion channels and used time-resolved photobleaching to determine the stoichiometry of the NMDAR (2NR1:2NR3B); this was confirmed by verification of known stoichiometries of 2NR1:2NR2B and 3CNGA1:CNGA2 (37).

As the Dougherty and Lester labs have started studying neuronal nAChRs and γ-aminobutyric acid receptors (GABARs), subunit stoichiometry has become a concern. In this research, we hoped to use the known stoichiometry of the mouse muscle nAChR (2α:β:γ:δ) and try to attain this stoichiometry by densiometric analysis of Western blots. Using subunits containing the HA tag in the M3-M4 loop, it was hoped that the HA antibody would bind similarly to each subunit and insertion of nine amino acids (HA tag) would not perturb ion channel function as much as ≈ 240 amino acids for GFP. Previous work has shown that the nAChR subunits degrade rapidly when not assembled in ion channel complexes (27,28,38). We hoped that by using whole cells and looking at the total amount of each subunit protein, we would be able to determine the subunit ratio of the nAChR and apply this technology to the neuronal nAChRs and GABARs.

6.2 Results

6.2.1 Screening Sites For Aminoacylation of tRNAs, Read-Through, and UAA Incorporation

We chose to screen αD70 and aligned sites in the mouse muscle nAChR (Figure 6.1). These sites were chosen because the large UAA biocytin could be incorporated efficiently at αD70 and subsequently labeled with streptavidin without a significant shift in EC_{50} (39). αD70 is part of the main immunogenic region (MIR) of the nAChR, and this region binds many antibodies, including those associated with myasthenia gravis (a human autoimmune disease) (40,41). The αD70 site can therefore tolerate a large UAA, detection by streptavidin and antibodies shows the region is highly accessible, and should be accessible to small molecule, bioorthogonal reporters. The cryo-EM images of the *Torpedo* nAChR subsequently followed the biochemical work and clearly shows that MIR is highly exposed (Figure 6.1) (42). The αD70 aligned sites were chosen because it was hoped that these sites would incorporate UAAs efficiently and allow for multiple UAA incorporation for fluorescent resonance energy transfer (FRET) experiments. The βA19' site was also chosen because mutating this site to Cys allows for labeling when the nAChR is in the open state (43) and the site tolerates the incorporation of a large fluorescent UAA, Lys(BODIPYFL) (44).

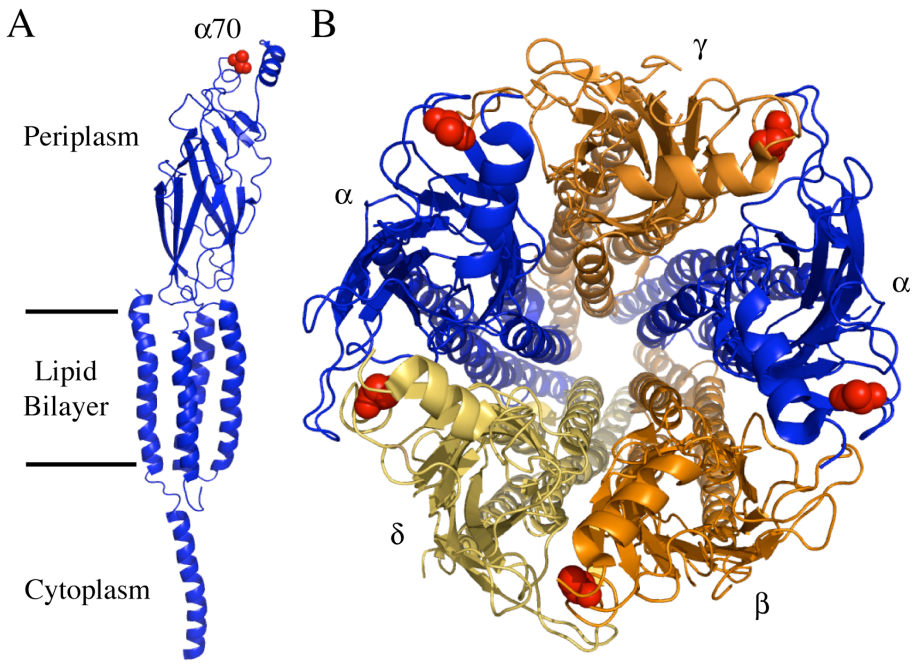

Figure 6.1: α70 and aligned positions in the nAChR. (A) The α-subunit of the nAChR is shown with the lipid bilayer as a reference. αD70 is shown in the extracellular domain in red. Incorporation of the UAA biocytin allows for labeling with radioactive streptavidin (39). This residue is part of the MIR and accessible to antibodies. (B) A top view of the nAChR with the residues aligned with αD70 shown in red. The amino acids at these positions are as follows: βA70, γK70, and δN70 in the mouse muscle nAChR (residues shown are from the *Torpedo* nAChR). Image created from 2BG9.pdb (42).

In order to screen the selected sites, the amber (UAG), opal (UGA), and quadruplet (GGGU) codons were utilized to prepare for multiple UAA incorporation. THG73 is an amber suppressor tRNA used extensively to incorporate UAAs in *Xenopus* oocytes (45–47). THG73 is aminoacylated with Gln in *Xenopus* oocytes when incubated for > 1 day and large quantities of tRNA are used (48,49). TQAS is an amber suppressor tRNA created from THG73 by the placement of four mutations in the acceptor stem (shown in Figure 4.3), is aminoacylated much less than THG73, and shows similar suppression efficiency in *Xenopus* oocytes from Nasco (48,50). TQAS' is an amber suppressor tRNA created from THG73 by the placement of five mutations in the acceptor stem (shown in Figure 4.3), is aminoacylated comparably to THG73, and shows similar

suppression efficiency in *Xenopus* oocytes from Nasco (48,50). $YFaFS_{ACCC}$ is a frameshift suppressor tRNA (shown in Figure 3.2) shown to be the most orthogonal suppressor tRNA tested in *Xenopus* oocytes, but has a suppression efficiency of ≈ 30% when compared to the amber suppressor tRNAs (48–50). TQOpS' is an opal suppressor tRNA created from THG73 by the placement of five mutations in the acceptor stem and containing the anticodon UCA (shown in Figure 4.3), is aminoacylated much less than THG73, and is capable of incorporating an UAA (48,50).

Table 6.1 shows aminoacylation of tRNAs, read-through, and UAA incorporation experiments at the selected sites (experimental concept discussed in Chapter 4 and shown in Figure 4.1). In the experiments, THG73 was added in large quantities and incubated for 2 days in order to obtain aminoacylation with Gln *in vivo*. Any site that could incorporate a large UAA should also incorporate Gln. For UAA incorporation, 5-F-Tryptophan (WF1) (chemical structure in Figure 3.2) was chemically ligated to the suppressor tRNA.

α70UAG shows large aminoacylation product when incubated with THG73, but this aminoacylation product is reduced when incubated with TQAS (Table 6.1). α70UAG mRNA injected alone shows little read-through of the UAG stop codon (Table 6.1) and therefore this site is optimal for the incorporation of UAAs. β70UAG and β70GGGU show extremely large read-through when mRNA is injected alone, which is very rare, and therefore this site is not useful for UAA incorporation (Table 6.1). THG73 is aminoacylated similarly to TQAS' at β70UAG in Nasco oocytes (Table 6.1). TQAS and $YFaFS_{ACCC}$ are aminoacylated much less and close to the β70XXX(X) mRNA alone (Table 6.1). Interestingly, TQAS'-WF1 shows a 180% increase in current compared to

THG73 (Table 6.1) and shows that UAA incorporation by the chemically aminoacylated tRNA is much more efficient at producing functional channels than THG73 being aminoacylated with Gln *in vivo*, which is in agreement with previous experiments (45,48). The β19'XXX(X) position shows large amounts of read-through with large quantities of mRNA injected alone, but much less than the β70 position (Table 6.1). THG73 also shows a reduction of ≈ 79% in current when tested at β19'UAG when compared to β70UAG (Table 6.1). TQAS and $YFaFS_{ACCC}$ also show larger amounts of aminoacylation, relative to THG73, at the β19' position when compared to the β9' position (see Chapter 4 and (48,49)). Therefore the β19' position is not optimal for UAA and requires the use of less mRNA to avoid read-through and use of orthogonal tRNAs to avoid aminoacylation signals that can be comparable to suppression, which has been done experimentally for the incorporation of a fluorescent UAA (44).

δ69 experiments show little current with suppressor tRNAs that are not chemically aminoacylated and with the injection of mRNA only (Table 6.1). THG73 injected with δ69UAG is comparable to mRNA only, indicating that the site doesn't tolerate the incorporation of Gln (Table 6.1). The δ69 position is not useful for the incorporation of UAAs. δ70UGA also shows very little current with the injection of TQOpS', TQOpS'-WF1, and mRNA alone (Table 6.1). Intriguingly, there is an 80% reduction in current when TQOpS'-WF1 is injected relative to TQOpS', which is not chemically aminoacylated, (Table 6.1) and shows that WF1 is not tolerated at δ70UGA. The δ70UGA position is not optimal for incorporation of UAAs. The optimum site screened was α70UAG because it showed very little read-through when mRNA alone

was injected and low aminoacylation currents were obtained with TQAS. α70UAG was therefore chosen for further experiments.

Table 6.1: Expression tests at the αD70 aligned positions and βA19'.

mRNA	**tRNA**	**Norm**	**n** [a]
α70UAG	THG73	1.0 [b]	16
α70UAG	TQAS	0.27	15
α70UAG		0.017	16
β70UAG	THG73	1.0 [c]	16
β70UAG	THG73-dCA	1.0 [d]	11
β70UAG	TQAS'-dCA	1.1	12
β70UAG	TQAS	0.40	12
β70UAG	TQAS'-WF1	2.8	12
β70UAG		0.31	14
β70GGGU	$YFaFS_{ACCC}$	0.41	15
β70GGGU		0.40	16
β19'UAG	THG73	1.0 [e]	16
β19'UAG	TQAS	0.36	15
β19'UAG		0.23	16
β19'GGGU	$YFaFS_{ACCC}$	0.24	16
β19'GGGU		0.14	16
δ69UAG	THG73	1.0 [f]	16
δ69UAG	TQAS	0.82	16
δ69UAG		0.92	16
δ69GGGU	$YFaFS_{ACCC}$	0.64	15
δ69GGGU		1.0	16
δ70UGA	TQOpS'-dCA	1.0 [g]	7
δ70UGA	TQOpS'-WF1	0.20	7
δ70UGA		0.54	6

[a] Number of oocytes tested.
[b] Average I_{max} = -19 μA
[c] Average I_{max} = -15 μA
[d] Average I_{max} = -13 μA
[e] Average I_{max} = -2.9 μA
[f] Average I_{max} = -0.26 μA
[g] Average I_{max} = -0.31 μA

6.2.2 Suppression of α70UAG with TQAS-Biocytin

In order to directly detect an UAA incorporated into the nAChR by Western blot, large amounts of protein are needed, which usually requires multiple injections, large amounts of tRNA-UAA, choosing only oocytes that are expressing > 10 μA, and removing membranes from 10–25 oocytes for each gel lane (51,52). Multiple injections are not optimal because oocyte death increases with the number of injections and requires large amounts of tRNA-UAA. Manually removing membranes from oocytes is also tedious and time consuming for a large number of samples and variability can arise from incomplete removal of the membrane. For the following Western blots, saturating amounts of TQAS-Biocytin were prepared and only a single injection was performed with large amounts of mRNA. Biocytin is a difficult UAA to incorporate *in vitro* and *in vivo* (39,53), but the average maximal current obtained from a single injection of α70UAG + TQAS-Biocytin was -10.4 μA (23% relative to wild-type current with half the mRNA), which is more than sufficient for detection by Western blot. Whole-cell detection of an UAA was also explored because it requires fewer oocytes for each lane, is not as time consuming, and there is less variability.

Figure 6.2 shows detection of α70Biocytin using four whole oocytes (Figure 6.2, A & B) or twenty oocyte membranes (Figure 6.2, C & D). The Western blots show that many endogenous proteins are biotinylated in uninjected *Xenopus* oocytes (Figure 6.2, A, Lanes 2–4, and Figure 6.2, C, Lanes 2–4), but the endogenous proteins don't overlap with the α-subunit of the nAChR (Figure 6.2, B & D). Using four oocytes per lane, the UAA biocytin can be detected in three separate samples (Figure 6.2, A, Lanes 5–7), and no band is observed at the same molecular weight for uninjected oocytes (Figure 6.2, A,

Lanes 2–4) or wild-type nAChR (Figure 6.2, A, Lanes 8–10). The α-subunit is clearly detected using the HA tag with four whole cells for α70Biocytin and for the wild-type nAChR (Figure 6.2, B, Lanes 5–10). By the whole-cell Western blot, the suppression efficiency of TQAS-Biocytin at α70UAG is 8.7% relative to the wild-type nAChR, which is not an ideal comparison because the wild-type nAChR has only half the mRNA of the suppression experiment.

Manually removing the oocyte membranes shows decreased amounts of endogenous biotinylated proteins (Figure 6.2, C, Lanes 2–10) and therefore most of the biotinylated proteins are not associated with the membrane surface. α70Biocytin is clearly visualized only in the membrane preparation (Figure 6.2, C, Lane 7) and there is no α70Biocytin detected in the supernatant (Figure 6.2, C, Lanes 5–6). The α-subunit is clearly visualized in the membrane preparation of both α70Biocytin and the wild-type nAChR (Figure 6.2, D, Lanes 7 & 10), but the α-subunit is also visible in the supernatant of the wild-type nAChR (Figure 6.2, D, Lanes 8–9). This is most likely caused by the presence of 0.07% SDS in the hypotonic solution used to remove the oocyte membranes and may only be visible in the wild-type nAChR due to the large amount of α-subunit present. By manually removing the membrane of the oocytes, the suppression efficiency of TQAS-Biocytin at α70UAG is 58% relative to wild-type nAChR, which has half the amount of mRNA. Overall the Western blots of the whole cell homogenization and manually removed membranes are comparable, but α70Biocytin shows a stronger signal in the whole cell preparation with only four cells (Figure 6.2, A, Lanes 5–7) compared to the signal from biocytin from twenty manually removed membranes (Figure 6.2, C, Lane 7). Therefore, whole-cell homogenization was used for the remainder of the Western

blots because of stronger signal, ease of experiments, and to avoid loss of protein that can cause variability.

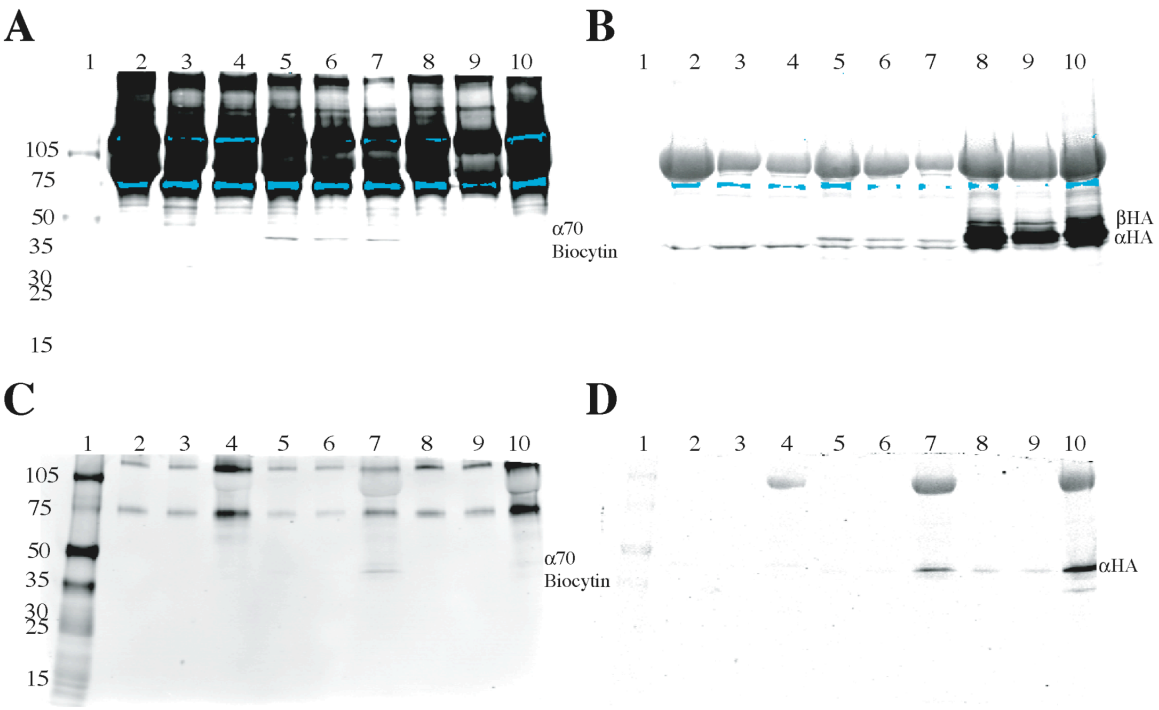

Figure 6.2: Detection of α70Biocytin by Western blot. (A) Whole-cell detection of α70Biocytin. (B) Whole-cell detection of HA tag. (A & B) Lane 1, molecular weight maker. Lanes 2–4, uninjected oocytes. Lanes 5–7, are α_{NHA}70UAG + TQAS-Biocytin. Lanes 8–10 are α_{HA} and β_{HA}. Each lane contains four homogenized oocytes. Blue bands in A and B represent pixels saturated by detection with Streptavidin-680. (C) Membrane detection of α70Biocytin. (D) Membrane detection of HA tag. (C & D) Lane 1, molecular weight marker. Lanes 2 and 3, supernatant of uninjected oocytes. Lane 4, membrane preparation of uninjected oocytes. Lanes 5 and 6, supernatant of α_{NHA}70UAG + TQAS-Biocytin. Lane 7, membrane preparation of α_{NHA}70UAG + TQAS-Biocytin. Lanes 8 and 9, supernatant of α_{HA}. Lane 10, membrane preparation of α_{HA}. Twenty oocyte membranes were manually stripped in a low detergent, hypotonic solution and placed in an eppendorf. Membranes were pelleted by centrifugation and the supernatant is the soluble fraction. Numbers on the left are molecular weight markers (KD).

6.2.3 Analysis of ^{125}I-Streptavidin and ^{125}I-α-Bungarotoxin Binding to *Xenopus* Oocytes Expressing Wild-Type nAChR and UAA Incorporation of Biocytin

Previous experiments identified significant binding of ^{125}I-Streptavidin to oocytes expressing α70UAG + THG73-Biocytin, but there was a lack of significant binding to α76UAG + THG73-Biocytin (39). Using Dr. Justin Gallivan's lab notebook, I reanalyzed all of the experiments performed to gain further insights on the amount of endogenous biotinylated protein on the *Xenopus* oocyte surface and to obtain information on unpublished results. All experiments were performed previously by Dr. Gallivan and unfortunately the health of the oocytes and expression of nAChR with different batches of oocytes was not always available.

Figure 6.3 shows the analysis of ^{125}I-Streptavidin and ^{125}I-α-Bungarotoxin binding to oocytes expressing wild-type nAChR, mRNA with the amber (UAG) codon at the site of interest, incorporation of natural amino acids or UAAs by nonsense suppression, and biocytin incorporated at various positions. Data are given as a ratio of the average signal of the tested sample divided by the average signal of the blank. Figure 6.3 shows there is ≈ 2-fold increase in signal when ^{125}I-Streptavidin is used to label uninjected oocytes, oocytes injected with mRNA only, and mRNA + THG73 (dCA or dCA-X, where X is Tyr, *p*-AcPhe, or ketoTyr). The suppression of THG73-Biocytin at all positions other than α70UAG showed no significant increase in radioactive signal (Figure 6.3, orange bar, left), in agreement with published experiments (39). Only suppression of α70UAG + THG73-Biocytin resulted in significant radioactive signal (Figure 6.3), which is also in agreement with published experiments (39). Therefore, endogenous biotinylated proteins may be present on the extracellular membrane of *Xenopus* oocytes, as shown by the

increase in radioactive signal, or this may be due to nonspecific binding of ^{125}I-Streptavidin to the membrane surface.

Two ^{125}I-α-Bungarotoxin molecules are expected to bind a single nAChR receptor because there are two α-subunits (54). The labeling of ^{125}I-α-Bungarotoxin and ^{125}I-Streptavidin is similar on uninjected oocytes (Figure 6.3, red bars) even though ≈ 3 times greater concentration was used for ^{125}I-α-Bungarotoxin labeling (39). Intriguingly, the ^{125}I-α-Bungarotoxin radioactive signal is increased for all injections and there is a greater difference over uninjected oocytes when compared to ^{125}I-Streptavidin labeling (Figure 6.3). mRNA only (for all sites tested in (39)) shows an increase in ^{125}I-α-Bungarotoxin binding and suggests that the read-through product is accessible on the surface and in agreement with electrophysiology data for α70UAG shown in Table 6.1. mRNA + THG73-dCA also shows a significant increase in labeling and is in agreement with functional channels on the surface (Table 6.1). Incorporation of *p*-AcPhe, ketoTyr, or Tyr by THG73 results in the highest labeling and shows the average suppression efficiency at various sites is much greater than THG73-Biocytin at various sites (Figure 6.3, right, light-green bar compared to orange bar). α70UAG + THG73-Biocytin shows robust binding of ^{125}I-α-Bungarotoxin, but suppression of THG73-Biocytin at other sites shows little channel expression by electrophysiology (39) and no statistical difference of ^{125}I-α-Bungarotoxin labeling over uninjected oocytes (Figure 6.3, right, orange bar compared to red bar).

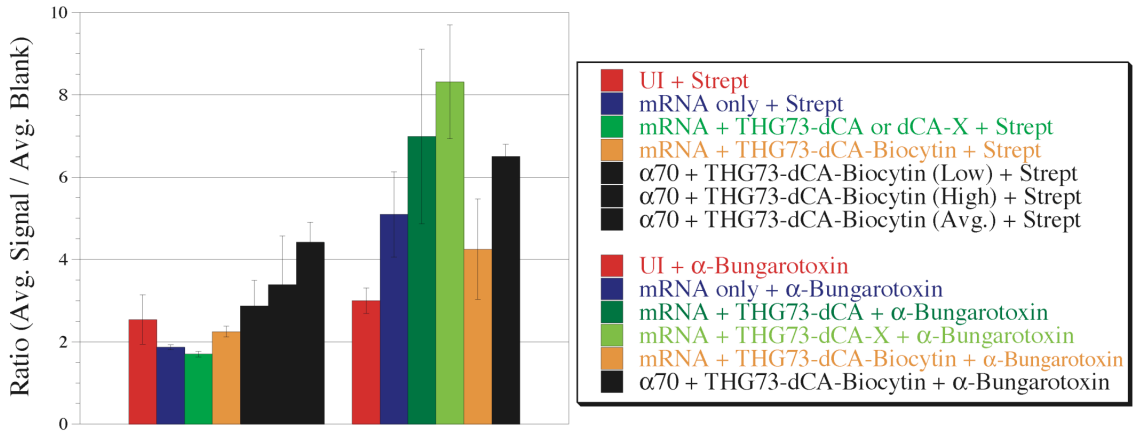

Figure 6.3: Analysis of ^{125}I-Streptavidin or ^{125}I-α-Bungarotoxin labeling of *Xenopus* oocytes expressing wild-type nAChR and UAA incorporation of biocytin. Abbreviations: UI is uninjected oocytes; Strept is ^{125}I-Streptavidin; mRNA refers to any other suppression site other than α70UAG; THG73-dCA is the 76mer tRNA; THG73-dCA-X is THG73 ligated with Tyr, *p*-AcPhe, or ketoTyr (shouldn't bind ^{125}I-Streptavidin); THG73-dCA-Biocytin is THG73-Biocytin; α70 is α70UAG, (Low) is the lowest avg. I_{max} in an oocyte batch; (High) is the highest avg. I_{max} in an oocyte batch; (Avg.) is when oocytes were labeled without determining the avg. I_{max}; and α-Bungarotoxin is ^{125}I-α-Bungarotoxin.

6.2.4 Bioorthogonal Labeling of α70*p*-AcPhe With Biotin Hydrazide

The incorporation of *p*-AcPhe at α70 introduces a ketone on the surface of *Xenopus* oocytes (Figure 6.1), which can be labeled with hydrazides. The ketone is bioorthogonal only on the cell surface because the interior of the cell contains acetylated proteins and keto/aldehydic metabolites (1). The desired bioorthogonal reaction of *p*-AcPhe with biotin hydrazide, which is membrane impermeant, is shown in Figure 6.4. *p*-AcPhe was incorporated at α70UAG using TQAS and showed an average maximal current of -27.3 μA (61% relative to wild-type current with half the mRNA), which is ≈ 3-fold greater when compared to TQAS-Biocytin incorporation. To analyze the reaction of biotin hydrazide with *p*-AcPhe, we chose Western blot detection because α70Biocytin and α70Biocytin bound to streptavidin showed little shift in EC_{50} (39) and Western blot allows for visualization of all protein bands labeled with biotin hydrazide.

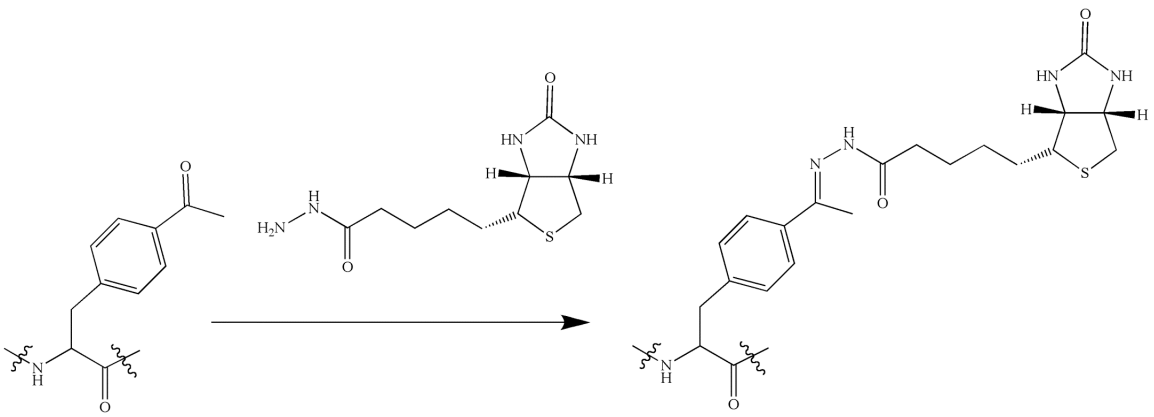

Figure 6.4: Bioorthogonal labeling of *p*-AcPhe with biotin hydrazide. *p*-AcPhe is incorporated at α70 and expressed on the extracellular surface of the *Xenopus* oocyte (Figure 6.1). The cells are labeled with biotin hydrazide, which can't cross the cell membrane unless it is permeabilized. The hydrazide reacts with the ketone to produce a hydrazone and covalently attaches biotin to *p*-AcPhe.

Labeling of α70*p*-AcPhe with biotin hydrazide is shown in Figure 6.5. Labeling of permeabilized, uninjected oocytes and permeabilized, α70UAG + TQAS-*p*-AcPhe with biotin hydrazide results in detection of many proteins with Streptavidin-680 (Figure 6.5, A, Lanes 4 & 7), which is more intense than non-permeabilized oocytes (Figure 6.5, A, Lanes 3 & 6). α70*p*-AcPhe shows no labeling above the uninjected oocytes (Figure 6.5, A, Lanes 3 & 6). α70*p*-AcPhe shows greater α-subunit signal (Figure 6.5, B, Lane 5) than α70*p*-AcPhe labeled with biotin hydrazide (Figure 6.5, B, Lane 6). The reaction of ketones with hydrazides is pH sensitive and optimum in the range of pH = 4–6.5 (1,6,10,13,19). Therefore biotin hydrazide labeling of α70*p*-AcPhe was tested from pH = 4–7.5 (Figure 6.5, C). Biotin hydrazide labeling of α70*p*-AcPhe shows three distinct protein bands when the pH = 4–6.6 (Figure 6.5, C, Lanes 4–9). Intriguingly, varying pH also alters protein translation of the α70*p*-AcPhe subunit, which is optimum at pH = 6.3–7.5 (Figure 6.5, D, Lanes 8–10) and is severely decreased at pH = 4 (Figure 6.5, D, Lanes 3–4).

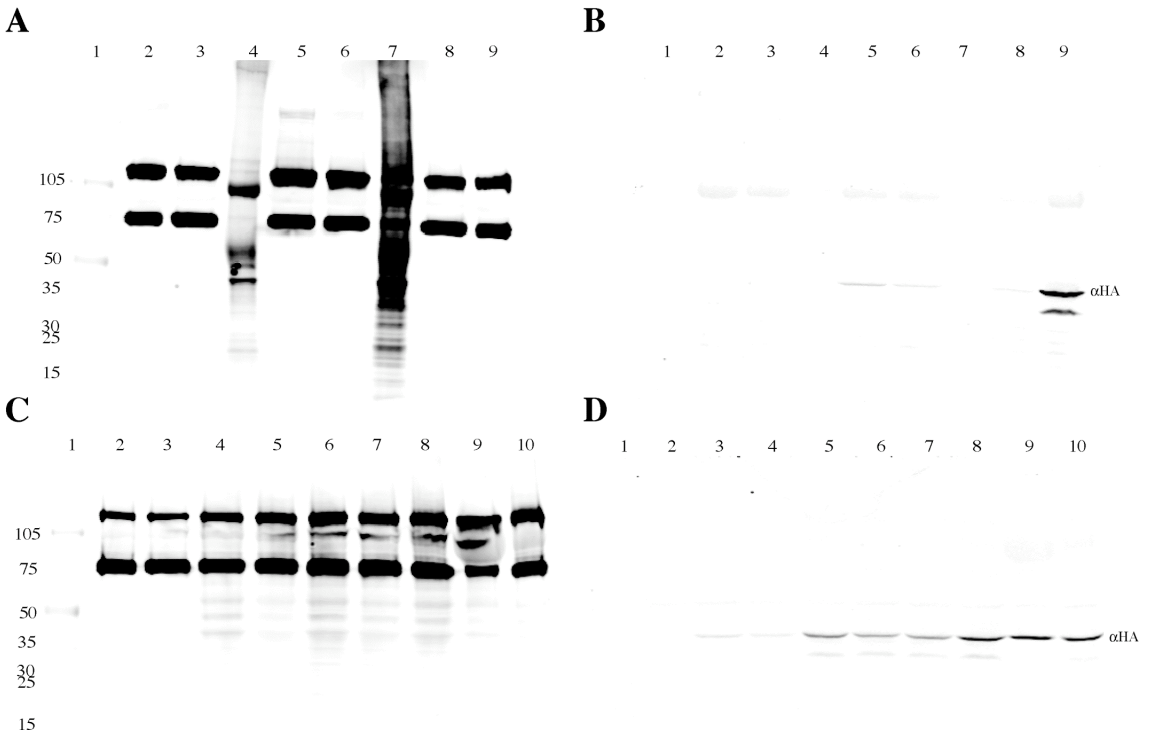

Figure 6.5: Detection of α70*p*-AcPhe labeled with biotin hydrazide. (A) Whole-cell detection of biotin hydrazide labeling of intact and permeabilized oocytes. (B) Detection of the HA tag. (A & B) Lane 1, molecular weight marker. Lane 2, uninjected oocytes. Lane 3 is uninjected oocytes labeled with 1 mM biotin hydrazide, pH = 7.5. Lane 4 is uninjected oocytes permeabilized with detergent and labeled with 1 mM biotin hydrazide, pH = 7.5. Lane 5 is α_{NHA}70UAG + TQAS-*p*-AcPhe. Lane 6 is α_{NHA}70UAG + TQAS-*p*-AcPhe labeled with 1 mM biotin hydrazide, pH = 7.5. Lane 7 is α_{NHA}70UAG + TQAS-*p*-AcPhe permeabilized with detergent and labeled with 1 mM biotin hydrazide, pH = 7.5. Lane 8 is uninjected oocytes. Lane 9 is α_{HA}. (C) Whole-cell detection of biotin hydrazide labeling of intact oocytes with different pH. (D) Detection of α_{NHA}. (C & D) Lane 1, molecular weight marker. Lane 2 is uninjected oocytes labeled with 1 mM biotin hydrazide, pH = 4. Lane 3, α_{NHA}70UAG + TQAS-*p*-AcPhe, pH = 4. Lane 4, α_{NHA}70UAG + TQAS-*p*-AcPhe labeled with 1 mM biotin hydrazide, pH = 4. Lane 5, α_{NHA}70UAG + TQAS-*p*-AcPhe labeled with 1 mM biotin hydrazide, pH = 4.6. Lane 6, α_{NHA}70UAG + TQAS-*p*-AcPhe labeled with 1 mM biotin hydrazide, pH = 5.3. Lane 7, α_{NHA}70UAG + TQAS-*p*-AcPhe labeled with 1 mM biotin hydrazide, pH = 5.8. Lane 8, α_{NHA}70UAG + TQAS-*p*-AcPhe labeled with 1 mM biotin hydrazide, pH = 6.3. Lane 9, α_{NHA}70UAG + TQAS-*p*-AcPhe labeled with 1 mM biotin hydrazide, pH = 6.6. Lane 10, α_{NHA}70UAG + TQAS-*p*-AcPhe labeled with 1 mM biotin hydrazide, pH = 7.5. Each lane contains four whole oocytes. Numbers on the left are molecular weight markers (KD).

Densiometric analysis of α70*p*-AcPhe labeled with biotin hydrazide at different pH is shown in Figure 6.6. Significant labeling is seen from pH = 4–6.3 (Figure 6.6, A).

Labeling at pH = 4.6 is expected to be greater than pH = 5.3 and pH = 5.8 is expected to be greater than pH = 6.3. Labeling may be decreased by variability of labeling, protein expression, or oocytes (Figure 6.6, A). α-subunit expression at different pH shows a gradual decrease as acidity increases (Figure 6.6, B). Even though the α-subunit is severely diminished at pH = 4, the greatest labeling is seen at pH = 4 (Figure 6.6, A & B). Streptavidin-680 labeling was then normalized by the amount of protein detected by the HA antibody to allow for comparison of biotin hydrazide labeling as a function of pH alone (Figure 6.6, C). pH = 7.5 shows virtually no labeling, which is expected of an acid catalyzed reaction (Figure 6.6, C). pH = 4 is the optimum labeling condition, even though protein production is decreased significantly (Figure 6.6, C). All subsequent hydrazide labeling experiments were performed at pH = 4.

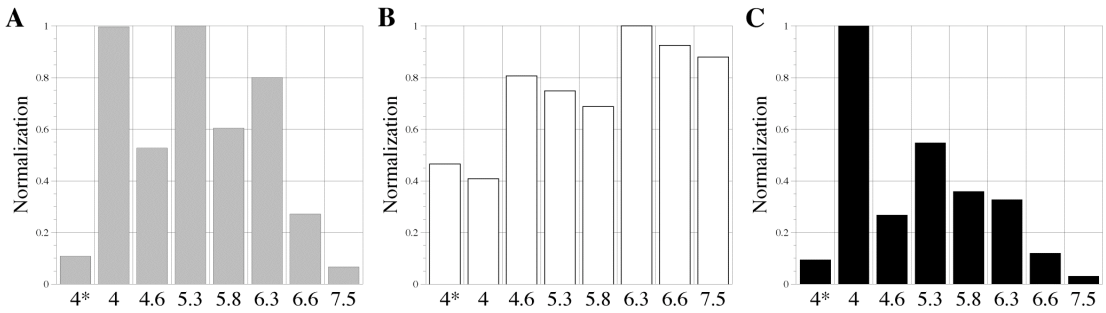

Figure 6.6: Analysis of *p*-AcPhe labeled with biotin hydrazide. Analysis performed on Western blots in Figure 6.5, C and D. (A) Densiometric analysis of biotin hydrazide labeling at different pH. Signals were normalized to the highest labeling (Figure 6.5, C, Lanes 2–10). (B) Densiometric analysis of protein expression as a function of pH. Signals were normalized to the highest expression (Figure 6.5, D, Lanes 2–10). (C) Normalization of biotin hydrazide labeling with the amount of protein expressed (value from A / value from B and renormalized to the highest value). Biotin hydrazide labeling is optimal at pH = 4, but protein translation is decreased. Numbers below each graph are pH. 4* was not labeled with biotin hydrazide.

6.2.5 Attempts to Block Nonspecific Biotin Hydrazide Labeling of Uninjected Oocytes

The labeling of three bands in Figure 6.5 is undesired because the reaction of biotin hydrazide is expected to be specific for the α70*p*-AcPhe. Therefore, carbohydrazide was added to uninjected oocytes to try and block proteins that are reacting with the biotin hydrazide (Figure 6.7, A). Treatment of uninjected oocytes with 1 mM or 10 mM carbohydrazide for 1 day (Figure 6.7, A, Lanes 5–10) shows no reduction in biotin hydrazide labeling when compared to untreated, uninjected oocytes labeled with biotin hydrazide (Figure 6.7, A, Lanes 3–4). Another possibility is that ketones or aldehydes exist on the cell surface by protein modification or glycosylation of proteins and these are reacting with the biotin hydrazide. $NaBH_4$ reduces ketones and aldehydes into alcohols, which would not react with biotin hydrazide. Treatment of uninjected oocytes with 1 mM or 10 mM $NaBH_4$ showed no significant reduction in biotin hydrazide labeling (Figure 6.7, B Lanes 5–10) when compared to the untreated, uninjected oocytes labeled with biotin hydrazide (Figure 6.7, B, Lanes 3–4). Treatment of oocytes with carbohydrazide or $NaBH_4$ showed no reduction in biotin hydrazide labeling on uninjected oocytes (Figure 6.7, A & B) and surprisingly showed little effect on oocyte health and survival.

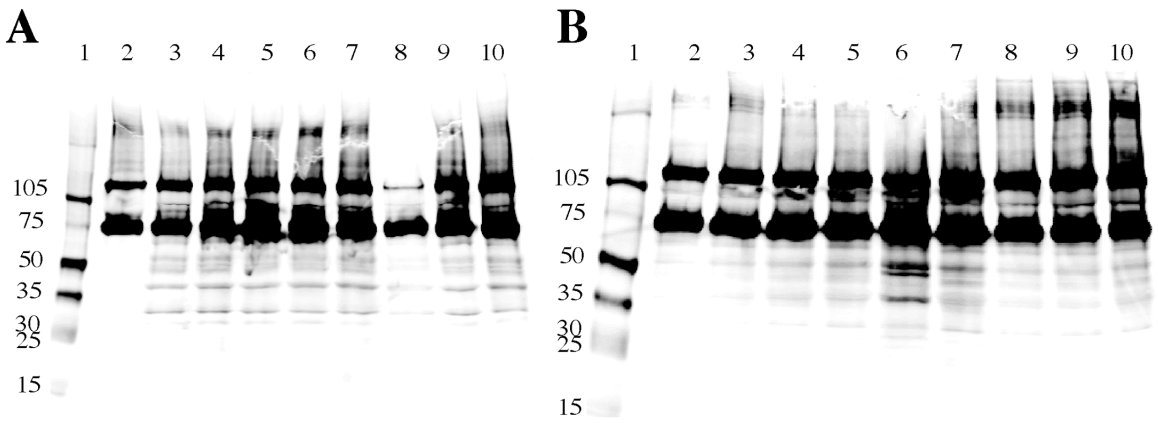

Figure 6.7: Uninjected oocytes labeled with biotin hydrazide after treatment with carbohydrazide or $NaBH_4$. (A) Carbohydrazide treatment prior to biotin hydrazide labeling. Lane 1 is molecular weight marker. Lane 2 is uninjected oocytes. Lanes 3 and 4 are uninjected oocytes labeled with 1 mM biotin hydrazide. Lanes 5–7, uninjected oocytes treated with 1 mM carbohydrazide, followed by labeling with 1 mM biotin hydrazide. Lanes 8–10, uninjected oocytes treated with 10 mM carbohydrazide, followed by labeling with 1 mM biotin hydrazide. (B) $NaBH_4$ treatment prior to biotin hydrazide labeling. Lane 1 is molecular weight marker. Lane 2 is uninjected oocytes. Lanes 3 and 4 are uninjected oocytes labeled with 1 mM biotin hydrazide. Lanes 5–7, uninjected oocytes treated with 1 mM $NaBH_4$, followed by labeling with 1 mM biotin hydrazide. Lanes 8–10, uninjected oocytes treated with 10 mM $NaBH_4$, followed by labeling with 1 mM biotin hydrazide. Each lane contains four oocytes and all labeling was performed at pH = 4. Numbers on the left are molecular weight markers (KD).

6.2.6 Bioorthogonal Labeling of α70*p*-AcPhe with Cy5.5 Hydrazide

Previous labeling experiments used biotin hydrazide, which contains the biotin moiety and could possibly be recognized by endogenous proteins and attached to proteins in order to sequester free biotin. Removing biotin from the environment is thought to be an antimicrobial mechanism used by avidin in egg whites and streptavidin in *S. avidinii* to inhibit microorganism growth (55). Therefore, it is possible that the *Xenopus* oocytes are removing the biotin hydrazide in a similar manner to inhibit microorganism growth. We then choose to label α70*p*-AcPhe with Cy5.5 hydrazide (structure shown in Figure 6.8, A) because the molecule doesn't resemble biologically active molecules and the infrared fluorophore would allow for direct detection by the Li-Cor Odyssey.

Labeling of uninjected oocytes, wild-type nAChR, and α70*p*-AcPhe with Cy5.5 hydrazide is shown in Figure 6.8, B. Permeabilized α70*p*-AcPhe labeled with Cy5.5 hydrazide show intense signals from many proteins (Figure 6.8, B, Lane 6), illustrating that many proteins within the cell can react with the Cy5.5 hydrazide and similar to biotin hydrazide (Figure 6.5, A, Lanes 4 & 7). Uninjected oocytes and oocytes expressing wild-type nAChR show three protein bands labeled by Cy5.5 hydrazide (Figure 6.8, B, Lanes 3 & 5). Three bands are also seen when labeling α70*p*-AcPhe (Figure 6.8, B, Lanes 7–8), which is similar to the labeling with biotin hydrazide (Figure 6.5, C, Lanes 4–9). Wild-type nAChR shows no reduction in protein when labeled with Cy5.5 hydrazide (Figure 6.8, C, Lanes 4–5). Labeling of α70*p*-AcPhe shows greatly diminished protein (Figure 6.8, C, Lanes 7–8) when compared to the untreated α70*p*-AcPhe (Figure 6.8, C, Lanes 9–10). This suggests covalent attachment of Cy5.5 hydrazide to α70*p*-AcPhe may be occurring and attachment of the large fluorophore is decreasing recognition by the HA antibody. However, there is still labeling of three protein bands and bioorthogonal labeling of the ketone doesn't appear to be a specific reaction on the surface of *Xenopus* oocytes.

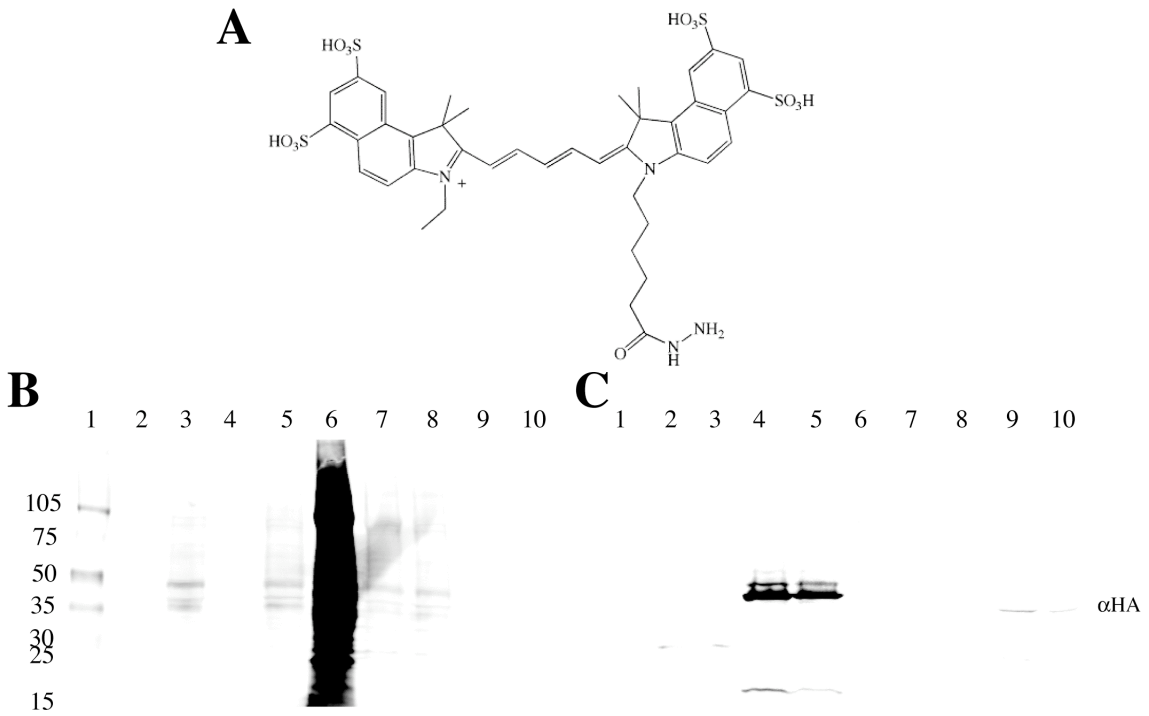

Figure 6.8: Bioorthogonal labeling of α70*p*-AcPhe with Cy5.5 hydrazide. (A) Chemical structure of Cy5.5 hydrazide. Maximal absorbance is 675 nm, maximal emission is 694 nm, and maximal extinction is 250,000 M^{-1} cm^{-1} (Amersham Biosciences product manual). Cy5.5 hydrazide allows for direct detection of labeled proteins. (B) Detection of Cy5.5 hydrazide labeled proteins. (C) Detection of the HA tag. (B & C) Lane 1 is molecular weight marker. Lane 2 is uninjected oocytes. Lane 3 is uninjected oocytes labeled with 1 mM Cy5.5 hydrazide. Lane 4 is α_{HA} and β_{HA}. Lane 5 is α_{HA} and β_{HA} labeled with 1 mM Cy5.5 hydrazide. Lane 6 is α_{NHA}70UAG + TQAS-*p*-AcPhe permeabilized with detergent and labeled with 1 mM Cy5.5. Lanes 7 and 8 are α_{NHA}70UAG + TQAS-*p*-AcPhe labeled with 1 mM Cy5.5 hydrazide. Lanes 9 and 10 are α_{NHA}70UAG + TQAS-*p*-AcPhe. Each lane contains four oocytes and all labeling and incubations were performed at pH = 4. Numbers on the left are molecular weight markers (KD).

6.2.7 Analysis of ^{125}I-Streptavidin Binding to *Xenopus* Oocytes Labeled with Biotin Hydrazide

Using Dr. Gallivan's lab notebook, I reanalyzed all experiments involving biotin hydrazide labeling (unpublished data). All experiments were performed previously by Dr. Gallivan using published methods (39). Oocytes expressing α70Biocytin show significant radioactive signal when labeled with ^{125}I-Streptavidin (Figure 6.9, black bar).

However, oocytes labeled with ≥ 0.5 mM biotin hydrazide (Figure 6.9, pink bar, light blue bars, & light green bars) show a similar radioactive signal to α70Biocytin (Figure 6.9, black bar). The labeling with biotin hydrazide is concentration dependent and 10 mM labeling of α70UAG + THG73-dCA or THG73-*p*-AcPhe/KetoTyr (Figure 6.9) shows comparable radioactive signal to nAChRs labeled with ^{125}I-α-Bungarotoxin (Figure 6.3). Therefore, the nonspecific labeling of biotin hydrazide is seen by Western blot (Figure 6.5 & 6.7) and also by ^{125}I-Streptavidin labeling of the oocyte surface (Figure 6.9).

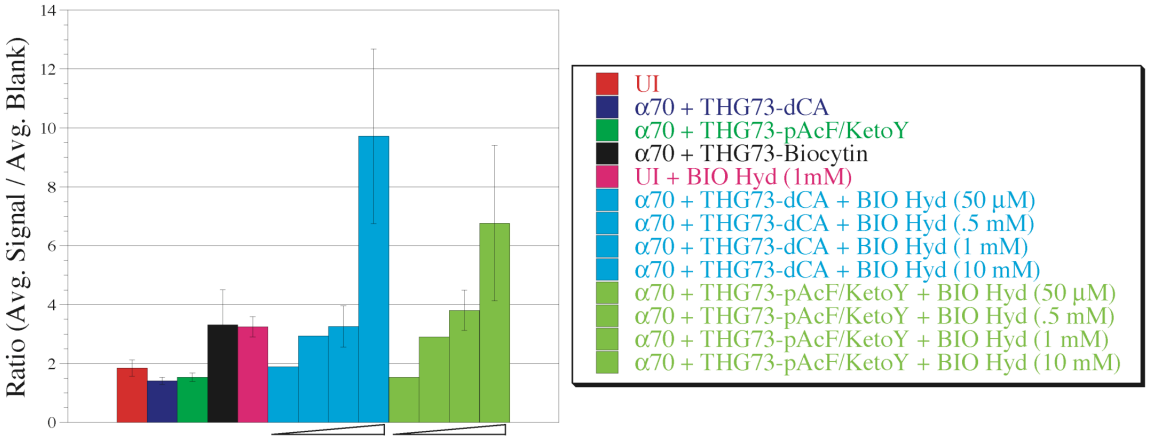

Figure 6.9: Analysis of ^{125}I-Streptavidin binding to *Xenopus* oocytes treated with biotin hydrazide. Abbreviations: UI is uninjected oocytes, α70 is α70UAG, THG73-dCA is the 76mer tRNA, THG73-dCA-pAcF/KetoY is THG73-*p*-AcPhe or THG73-KetoTyr, and BIO Hyd is biotin hydrazide, concentration shown in parentheses. Biotin hydrazide labeling is nonspecific and amplified with increasing concentrations.

6.2.8 α-, β-, γ-, and δ-Subunit Detection By Western Blot

Previously, Dr. Gabriel Brandt prepared the α-, β-, γ-, and δ-subunits containing the HA tag in the M3-M4 loop (denoted x_{HA} in contrast to the N-terminal HA tag, α_{NHA}). The M3-M4 loop is an intracellular loop that is highly flexible, can tolerate insertion of GFP (56), and can tolerate deletion of 108 amino acids in the 5-HT3A receptor and 75

amino acids in the GABAρ1 receptor (57). All subunits showed ≈ 100% expression, except the δ-subunit (≈ 90%), as determined by electrophysiology in *Xenopus* oocytes (58). We hoped that by using these constructs and the sensitivity of the Li-Cor Odyssey, we would be able to determine the subunit stoichiometry of the nAChR on whole oocytes. The subunit stoichiometry of the mouse muscle nAChR is known to be 2α:β:γ:δ (Figure 6.1) and this would allow for us to assay the feasibility of determining an ion channel stoichiometry on whole *Xenopus* oocytes by Western blot.

Figure 6.10 shows the expression of the α_{HA}, β_{HA}, γ_{HA}, and δ_{HA} constructs. The α_{HA}-subunit is clearly visible in all lanes (Figure 6.10, A & B). The β_{HA}-subunit is clearly visible on the 4–15% linear gradient gel (Figure 6.10, A, Lanes 4, 5, & 10), but is slightly obscured by the α_{HA} band on the 15% gel (Figure 6.10, B, Lanes 4–5). The γ_{HA}- and δ_{HA}-subunits are only slightly visible and smeared (Figure 6.10, A, Lanes 6–10 and Figure 6.10, B, Lanes 6–8 & 10). The δ_{HA}-subunit is only clearly visible in one lane (Figure 6.10, B, Lane 9). Western blot analysis of these constructs previously showed severely decreased signal for the non-α subunits (58), but the β_{HA}-subunit is clearly visible when the oocytes are expressing large amounts of protein (Figure 6.10, A, Lanes 4, 5, & 10).

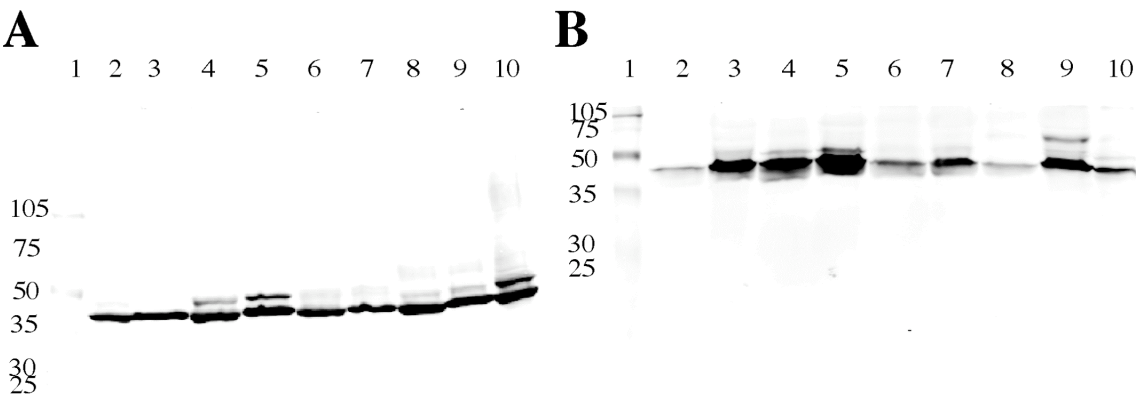

Figure 6.10: Detection of the α_{HA}, β_{HA}, γ_{HA}, and δ_{HA} subunits of the nAChR. (A) Subunit detection on a 4–15% linear gradient polyacrylamide gel. (B) Subunit detection on a 15% polyacrylamide gel. (A & B) Lane 1 is molecular weight marker. Lanes 2 and 3 are α_{HA}. Lanes 4 and 5 are α_{HA} and β_{HA}. Lanes 6 and 7 are α_{HA} and γ_{HA}. Lanes 8 and 9 are α_{HA} and δ_{HA}. Lane 10 is α_{HA}, β_{HA}, γ_{HA}, and δ_{HA}. Each lane contains four oocytes. Numbers on the left are molecular weight markers (KD).

6.2.9 α_{HA} and β_{HA} Detection After Various Incubation Times

In order to gain temporal information on protein translation of the α_{HA} and β_{HA} in *Xenopus* oocytes, the α_{HA} and β_{HA} were injected into oocytes and the whole-cell oocytes were homogenized at different time intervals after injection. Figure 6.11 shows the Western blot of different incubation times. Three hours after injection, only extremely little α_{HA}-subunit is seen (Figure 6.11, Lane 2). Six hours after injection, a slightly increased amount of α_{HA}-subunit is seen (Figure 6.11, Lanes 3–4). Twelve hours after injection, the α_{HA}-subunit is clearly visible (Figure 6.11, Lanes 5–6) and the β_{HA}-subunit is visible in only one lane (Figure 6.11, Lane 6). A day after injection, which is the typical minimum incubation time before electrophysiology, both the α_{HA} and β_{HA} subunits are clearly visible (Figure 6.11, Lanes 7–8). Two days after injection, there is increased amounts of both the α_{HA} and β_{HA}, clearly illustrating that protein translation has not saturated after two days.

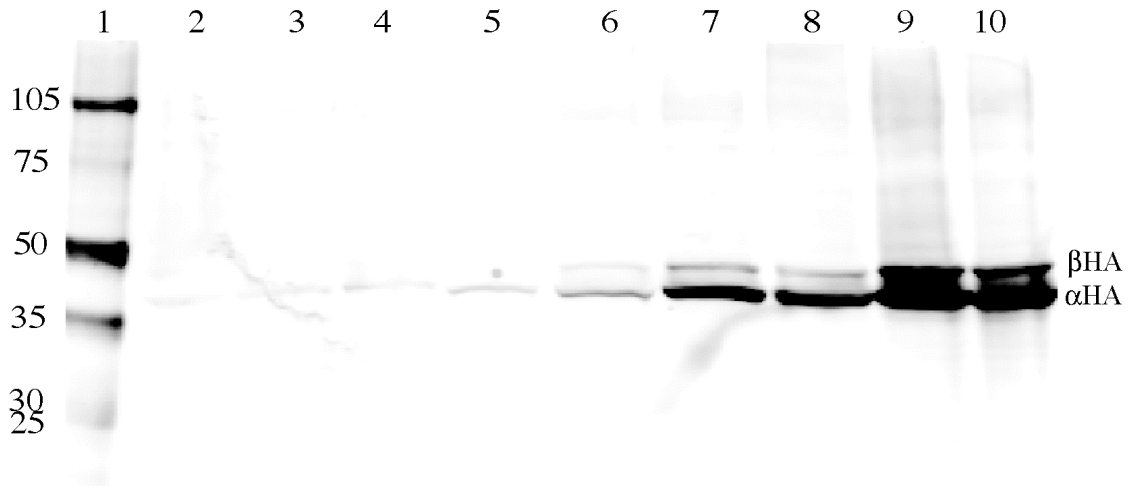

Figure 6.11: Detection of the α_{HA} and β_{HA} subunits at different incubation times. Lane 1 is molecular weight marker. Lane 2 is α_{HA} and β_{HA} 3 h after injection. Lanes 3 and 4 are α_{HA} and β_{HA} 6 h after injection. Lanes 5 and 6 are α_{HA} and β_{HA} 12 h after injection. Lanes 7 and 8 are α_{HA} and β_{HA} 24 h after injection. Lanes 9 and 10 are α_{HA} and β_{HA} 48 h after injection. Protein translation shows no saturation after 48 h. Each lane contains four oocytes. Numbers on the left are molecular weight markers (KD).

6.2.10 α_{HA} and β_{HA} Solubilization of Whole Cells or Insoluble Fraction

The nAChR is a membrane-associated ion channel and therefore may be difficult to solubilize in the presence of cytoplasmic proteins. In previous Western blots, whole cells were homogenized, all protein was solubilized, and samples were centrifuged to remove insoluble proteins, lipids, membrane, genomic DNA, etc. Cytoplasmic proteins were removed by homogenizing oocytes in ND96 buffer containing protease inhibitors, but no detergent. The samples were then centrifuged and the insoluble fraction was solubilized as done for the whole oocytes. Solubilization of the insoluble fraction greatly increases the yield of the α_{HA} and β_{HA} subunits (Figure 6.12, Lanes 6–9) when compared to the whole-cell homogenization (Figure 6.12, Lanes 2–5). The yield of the α_{HA} is increased 142%, while the β_{HA} is increased 108%. Therefore, homogenization of the insoluble fraction is useful for increased solubilization of the nAChR subunits and increased signal-to-noise when performing Western blots.

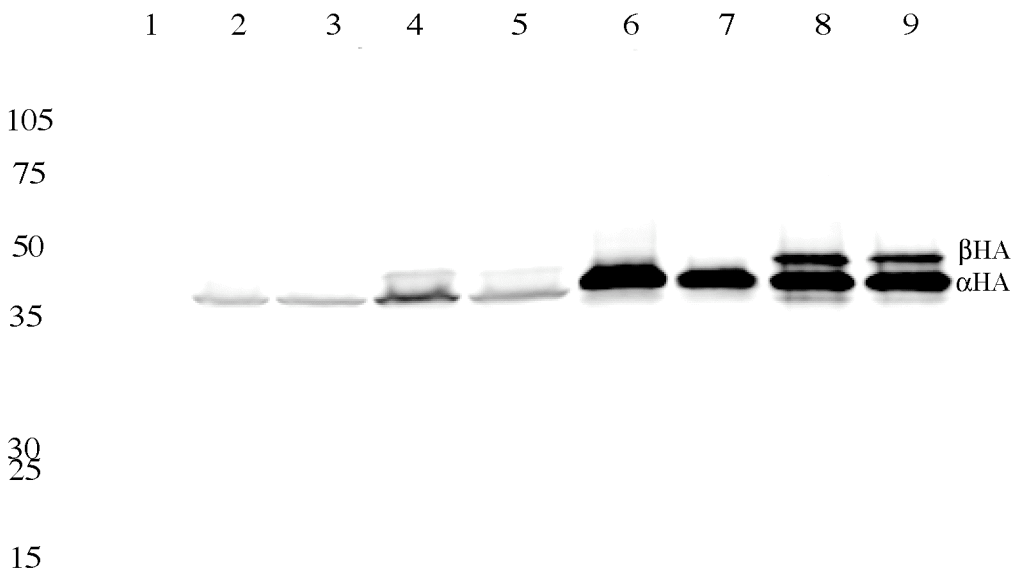

Figure 6.12: Increasing the yield of the α_{HA} and β_{HA} subunits. Lane 1 is molecular weight marker. Lanes 2 and 3 are α_{HA}. Lanes 4 and 5 are α_{HA} and β_{HA}. Lanes 6 and 7 are α_{HA} solubilized after cytoplasmic protein removal. Lanes 8 and 9 are α_{HA} and β_{HA} solubilized after cytoplasmic protein removal. Each lane contains four oocytes. Numbers on the left are molecular weight markers (KD).

6.2.11 α-, β-, γ-, and δ-Subunit Stoichiometry Determined By Densiometric Analysis

The densiometric analysis of all experiments is shown in Figure 6.13. The ratios were calculated by dividing the α_{HA} intensity by the intensity of the subunit expressed in the same lane. The expected ratio is 2 for all ratios in Figure 6.13 because the stoichiometry of the nAChR is 2α:β:γ:δ. The α/β average ratio is 2.9 ± 0.13 (Figure 6.13) and is the best ratio because the β_{HA} is clearly visible and is the average of 30 Western blot lanes or 120 oocytes. The α/γ average ratio is 2.9 ± 0.24 (Figure 6.13), which is similar to the α/β ratio even though the γ_{HA} band has decreased intensity compared to β_{HA}. The α/δ average ratio is 3.5 ± 0.51 (Figure 6.13) and is higher than the α/β or α/γ ratio. All ratios appear to indicate that there are ≈ 3 α-subunits for every β-, γ-

, and δ-subunit, which is in disagreement with the expected nAChR subunit stoichiometry.

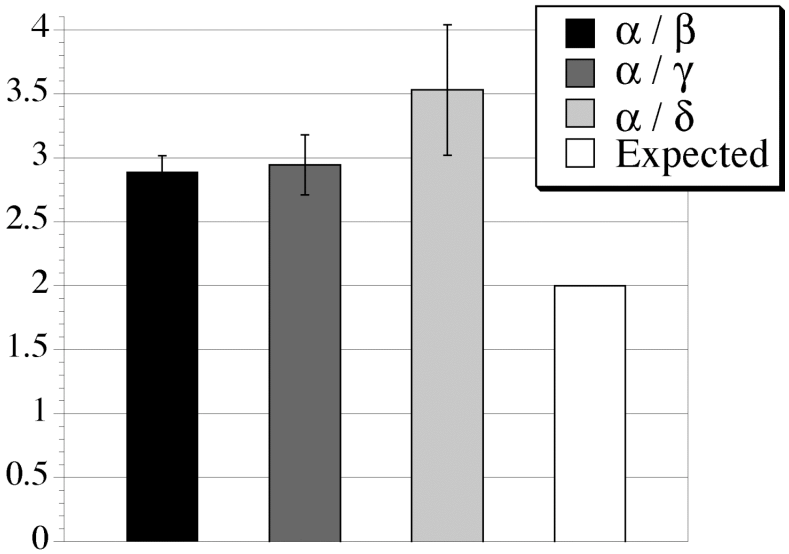

Figure 6.13: Average ratio of the β-, γ-, and δ-subunits relative to the α-subunit. The α/β ratio is an average of 30 lanes or 120 oocytes. The α/γ ratio is an average of 3 lanes or 12 oocytes. The α/δ ratio is an average of 3 lanes or 12 oocytes. The expected ratio is 2 by the nAChR stoichiometry being 2α:β:γ:δ.

6.3 Discussion

UAA incorporation is a useful technique for the introduction of novel chemical moieties, biophysical probes, and altered amino acid structures. However, efficient incorporation of large, bulky UAAs requires a suppression site that is tolerant, able to express well without altering protein folding and function, and doesn't have large amounts of read-through of the suppression site. Table 6.1 illustrates the differences between multiple suppression sites on different subunits of the nAChR. α70UAG incorporates Gln well with THG73 aminoacylated *in vivo* and shows little read-through of the stop codon (Table 6.1). β70UAG and β70GGGU both show large amounts of read-through (Table 6.1), even though a -1 frameshift at the GGGU quadruplet codon

presents multiple stop codons. TQAS'-WF1 shows a 180% increase in current when compared to THG73 not chemically aminoacylated (Table 6.1) and clearly illustrates that nonsense suppression with an UAA is more efficient that aminoacylation of THG73 *in vivo*. β19'UAG and β19'GGGU show increased amounts of read-through with large amounts of mRNA and less aminoacylation product than both α70UAG and β70UAG (Table 6.1). The β19' site is suboptimal for UAA incorporation and requires less mRNA to avoid read-through. δ69UAG, δ69GGGU, and δ70UGA all have very little read-through, but the aminoacylation of the suppressor tRNA doesn't significantly increase current (Table 6.1). δ70UGA + TQOpS'-WF1 has lower expression than mRNA alone or the aminoacylation product, clearly showing that the UAA is not tolerated at this site. Overall, the only optimum site is α70UAG for significant UAA incorporation without large amounts of read-through.

Western blot detection of UAAs has been exceedingly difficult because of the need for large amounts of protein on the oocyte surface, multiple injections of large quantities of tRNA-UAA, and manual removal of 10–25 oocyte membranes (51,52). Whole-cell homogenization of oocytes is a preferable alternative because the lack of manual membrane removal, decreased variability, and the need for only four oocytes. A single injection of large quantities of α70UAG + TQAS-Biocytin allowed for significant expression for Western blot detection (Figure 6.2, A & C). Figure 6.2 shows direct detection of the UAA biocytin incorporated at α70. Whole-cell homogenization shows increased intensity with four oocytes (Figure 6.2, A, Lanes 5–7) when compared to the traditional, manual membrane removal with twenty oocytes (Figure 6.2, C, Lane 7). Manual membrane removal requires a small amount of detergent in the hypotonic

solution, which causes loss of the α_{HA}-subunit in the supernatant (Figure 6.2, D Lanes 8–9). Whole-cell homogenization allows for increased intensity and fewer oocytes for each lane, so multiple experiments can be performed in a shorter amount of time. Solubilization of the insoluble fraction after removal of cytoplasmic proteins also increases the yield of the α_{HA} and β_{HA} subunits (Figure 6.12) and should further increase the signal-to-noise ratio in Western blot experiments.

Previous work has explicitly shown that there is protein translation saturation for luciferase after 3 h (59) or 12 h (60) with mRNA injection in *Xenopus* oocytes. However, Figure 6.11 clearly shows that protein expression is increasing for both the α_{HA} and β_{HA} subunits in the *Xenopus* oocytes, and no saturation is seen after 48 h. The experiment was performed using whole cell homogenization, which would solubilize α_{HA} and β_{HA} on the membrane surface, in vesicles, in the golgi, and in the endoplasmic reticulum. The increase in current with extended incubation time has been seen consistently within our lab, but it was unknown whether this was due to increased protein production or whether transport of ion channels from the endoplasmic reticulum to the cell surface was causing an increase in overall current. Figure 6.11 clearly shows that the α and β subunits are being expressed for at least 48 h from a single injection of wild-type mRNA.

α70UAG + THG73 shows large amount of current (Table 6.1) because THG73 is aminoacylated *in vivo* with Gln (48). TQAS is aminoacylated significantly less than THG73 in Nasco oocytes (Table 6.1 & (48)) and is useful for the incorporation of large amounts of biocytin and *p*-AcPhe. The incorporation of *p*-AcPhe is $\approx$ 200% more efficient than the incorporation of biocytin, which is most likely due to the large side chain of biocytin. Electrophysiology allows for detection of functional ion channels on

the surface of the oocyte membrane, which can often be produced by the desired UAA incorporation, or the undesired read-through of the suppression site or aminoacylation of the suppressor tRNA *in vivo* (Table 6.1). α-bungarotoxin is a snake venom toxin that irreversibly and competitively binds to the α-subunit of the nAChR in a region distinct from α70 (54,61), and the first 210 amino acids of the α-subunit (with no other subunits) is sufficient for α-bungarotoxin binding in *Xenopus* oocytes (62). Binding of ^{125}I-α-Bungarotoxin to oocytes is significant when incorporating biocytin, *p*-AcPhe, ketoTyr, and Tyr, but significant signal is also seen with mRNA only and with mRNA + THG73, which is not chemically aminoacylated (Figure 6.3). The significant radioactive signal agrees with large current seen with tRNA that are not chemically aminoacylated (Table 6.1). THG73, not chemically aminoacylated, with β9'UAG also produces large current (48,49,58) and the β9'Gln (aminoacylation product) has been detected by Western blot on the surface of *Xenopus* oocytes (58). Therefore, caution should be observed when labeling oocytes with α-bungarotoxin, because binding may not be limited to functional nAChRs, but also mutants, single α-subunits, and/or aminoacylation by products of UAA incorporation that may not be detected by electrophysiology.

Labeling of uninjected oocytes, wild-type nAChR, and α70UAG + TQAS-*p*-AcPhe with biotin hydrazide (Figure 6.5, C & Figure 6.7) or Cy5.5 hydrazide (Figure 6.8) show labeling of at least three protein bands that migrate near the α-subunit. Direct labeling of α70*p*-AcPhe with Cy5.5 hydrazide was not directly observed, but may be occurring due to the loss of α_{NHA} signal after labeling (Figure 6.8, C, Lanes 7–8), which was not seen in the unlabeled samples (Figure 6.8, C, Lanes 9–10). The nonspecific labeling with biotin hydrazide couldn't be prevented by treating uninjected oocytes with

carbohydrazide or $NaBH_4$ (Figure 6.7) and suggests that the labeled proteins contain an amino acid arrangement and/or glycosylation that is favorable for the reaction with the hydrazide chemical moiety. Previous work has labeled proteins containing the UAAs *p*-AcPhe and *m*-AcPhe with fluorescent hydrazides and biotin hydrazide *in vitro* and expressed in *E. coli* (13,19,20). Labeling of *E. coli* may not have nonspecific covalent attachment of hydrazides and/or the quantities of protein produced with UAAs is greater and gives a significant signal over background. In *Xenopus* oocytes, the ketone moiety does not appear to show site-specific labeling of α70*p*-AcPhe with biotin or Cy5.5 hydrazide and may only be useful for single ion channels studies involving FRET pairs.

Analyzing the subunit stoichiometry of the nAChR from whole oocytes shows ≈ 3 α-subunits for each non-α-subunit (Figure 6.13). Intriguingly, solubilizing the insoluble fraction gives an α/β ratio of 3.6 compared to whole-cell homogenization having an α/β ratio of 2.6 (data from analysis of Figure 6.12). The α/β ratio is 3.0 after 24 h incubation and the α/β ratio is 3.0 after 48 h incubation (data from analysis of Figure 6.11), which shows no variability in these two time points (the α/β ratio could not be calculated for 3, 6, and 12 h incubation because the signal was not above background). After injection of oocytes with α-subunit mRNA only, the α-subunit is expressed on the surface of *Xenopus* oocyte and can be detected by Western blot (58). Therefore, the oocytes can transport single α-subunits to the surface of the *Xenopus* oocyte that aren't in fully formed ion channels. The mouse α-subunit of the nAChR can also properly fold and have a high affinity α-bungarotoxin binding site when expressed alone in quail fibroblast cells (63). Notably, the α-subunit also has the slowest rate of degradation of all the subunits (38,63,64). The increased α_{HA} signal may also be caused by the injection of

mRNA in the subunit ratio of 2α:β:γ:δ, but this has been an established technique for many heteromeric ion channels expressed in *Xenopus* oocytes. Overall, subunit stoichiometry of the mouse muscle nAChR appears inaccurate using whole *Xenopus* oocytes and densiometric analysis of Western blots.

6.4 Experimental Methods

6.4.1 Materials

All oligonucleotides were synthesized by Integrated DNA Technologies (Coralville, IA). NotI and complete, EDTA-free protease inhibitor cocktail was from Roche Applied Science (Indianapolis). T4 RNA ligase and FokI were from NEB (Beverly, MA). T7 MEGAshortscript and T7 mMessage mMachine kits were from Ambion (Austin, TX). ACh chloride, biotin hydrazide, carbohydrazide, $NaBH_4$, and yeast inorganic pyrophosphatase were purchased from Sigma-Aldrich. HA.11 monoclonal antibody from mouse was from Covance (Berkeley, CA). Streptavidin conjugated to AlexaFluor680 and anti-mouse IgG from goat conjugated to AlexaFluor680 was from Molecular Probes (Eugene, OR). IRDye^{TM}800CW conjugated affinity purified anti-mouse IgG from goat was from Rockland (Gilbertsville, PA). Cy5.5 hydrazide was from Amersham Biosciences (Piscataway, NJ). dCA, 6-nitroveratryloxycarbonyl protected dCA-WF1, 6-nitroveratryloxycarbonyl protected dCA-Biocytin, and 6-nitroveratryloxycarbonyl protected dCA-*p*-AcPhe were prepared as reported (39,65–67).

6.4.2 tRNA Transcription and dCA or dCA-UAA Ligation

THG73, $YFaFS_{ACCC}$, TQAS, TQAS', and TQOpS' subcloned in the pUC19 vector were previously made (45,48–50). Template DNA for tRNA lacking the 3'CA

was prepared by FokI digestion and tRNA was transcribed using the T7 MEGAshortscript kit with 0.5 μl of yeast inorganic pyrophosphatase (40 U/ml in 75 mM Tris, 10 mM $MgCl_2$, and pH 7). tRNA was desalted using CHROMA SPIN-30 DEPC-H_2O columns (BD Biosciences) and concentration was determined by absorption at 260 nm. 75 μM of dCA (48,50) or 6-nitroveratryloxycarbonyl protected dCA-WF1/Biocytin/*p*-AcPhe were coupled to tRNA by using T4 RNA ligase for 30 min as previously reported (68,69), desalted using CHROMA SPIN-30 DEPC-H_2O columns, and quantified by absorption at 260 nm. tRNA ligation efficiency was qualitatively determined by MALDI mass spectrometry (69), and all tRNA ligations were > 90%.

6.4.3 nAChR Gene Preparation and mRNA Transcription

The masked α_{NHA}-, β-, γ-, and δ-subunits (all ending with the ochre (UAA) stop codon) of the nAChR subcloned in the pAMV vector were previously prepared (48,50). α70UAG, β70UAG, β70GGGU, β19'UAG, β19'GGGU, δ69UAG, δ69GGGU, and δ70UGA were prepared by QuikChange mutagenesis. Mutations were verified by DNA sequencing (California Institute of Technology Sequencing / Structure Analysis Facility). The α_{HA} (347), β_{HA} (365), γ_{HA} (365), and δ_{HA} (367) subunits all contain the HA tag in the M3-M4 intracellular loop and were previously prepared by Dr. Gabriel Brandt (58). DNA was linearized with NotI and mRNA was prepared with the T7 mMessage mMachine kit with 0.5 μl of yeast inorganic pyrophosphatase. mRNA was purified using the RNeasy Mini kit (Qiagen, Valencia, CA) and quantified by absorption at 260 nm.

6.4.4 *In Vivo* nAChR Expression Experiments

Prior to *in vivo* aminoacylation and suppression experiments, all tRNAs and mRNAs were simultaneously made and normalized by UV and densiometric analysis

using AlphaEaseFC Stand Alone (Alpha Innotech, San Leandro, CA). Stage VI oocytes of *Xenopus laevis* were prepared as described (70). All tRNAs were refolded at 65 ˚C for 2 min and 6-nitroveratryloxycarbonyl protected dCA-WF1/Biocytin/*p*-AcPhe was deprotected for 5 min by UV irradiation before injection (45). Oocytes were injected with 50 nl of mRNA alone or with tRNA and incubated at 18 ˚C for 44–52 h (unless otherwise stated in the Figure legends). 20 ng of mRNA in a subunit ratio of 10:1:1:1 for α70UAG:β:γ:δ; 2:5:1:1 for α:β70UAG:γ:δ, α:β70GGGU:γ:δ, α:β19'UAG:γ:δ, α:β19'GGGU:γ:δ; and 2:1:1:5 for α:β:γ:δ69UAG, α:β:γ:δ69GGGU, and α:β:γ:δ70UGA was injected in Table 6.1 with 10 ng of tRNA (when listed in Table 6.1). For TQAS-Biocytin and TQAS-*p*-AcPhe incorporation, 30 ng of mRNA (α70UAG:β:γ:δ) in a subunit ratio of 10:1:1:1 was injected with 100 ng of tRNA-UAA. 15 ng of mRNA (α:β:γ:δ) in a subunit ratio of 2:1:1:1 was injected for the wild-type nAChR.

6.4.5 Electrophysiology

Recordings employed two-electrode voltage clamp on the OpusXpress 6000A (Molecular Devices). ACh was stored at -20 ˚C as a 1 M stock, diluted in Ca^{2+}-free ND96, and delivered to oocytes by computer-controlled perfusion system. For all experiments, the holding potential was -60 mV. Suppression comparisons were tested with a single 1 mM ACh dose. Number of oocytes (*n*) is listed in Table 6.1.

6.4.6 Oocyte Labeling with Biotin Hydrazide and Cy5.5 Hydrazide

A 20 mM stock solution of biotin hydrazide was prepared in DMSO. 1 mM biotin hydrazide was prepared by adding 500 μl of 20 mM biotin hydrazide in DMSO (5% DMSO in final volume) to 9.5 ml ND96 with Ca^{2+} with no antibiotics and no horse serum added to avoid reaction with biotin hydrazide. When varying pH, the final

solution was adjusted using a pH meter and the pH is listed with each figure legend. A single oocyte (uninjected, α70UAG + TQAS-*p*-AcPhe, or α_{HA} and β_{HA}) was placed in a 1.5 ml eppendorf and labeled with 500 μl of 1 mM biotin hydrazide for > 20 h.

1 mg of Cy5.5 hydrazide was dissolved in 500 μl DMSO and added to 9.57 ml ND96 with Ca^{2+} (no antibiotics and no horse serum) pH = 4 to create 1 mM Cy5.5 hydrazide labeling solution. A single oocyte (uninjected, α70UAG + TQAS-*p*-AcPhe, or α_{HA} and β_{HA}) was placed in a 1.5 ml eppendorf and 500 μl of 1 mM Cy5.5 hydrazide solution was added. Oocytes were labeled for 22 h.

6.4.7 Oocyte Treatment with Carbohydrazide and $NaBH_4$

Carbohydrazide and $NaBH_4$ was dissolved in ND96 with Ca^{2+} (no antibiotics and no horse serum) pH = 4 to create 1 mM and 10 mM solutions immediately prior to treatment of cells. Single oocytes were placed in 1.5 ml eppendorfs and 500 μl of 1 mM or 10 mM of carbohydrazide or $NaBH_4$ was added. Oocytes were treated with carbohydrazide for 45 h and $NaBH_4$ for 24 h. Oocytes were subsequently labeled with 1 mM biotin hydrazide (as described in Section 6.4.6).

6.4.8 Whole Oocyte Homogenization and Membrane Preparation

Whole-cell homogenization was preformed by placing four oocytes (either immediately from 18 ˚C incubator or after storage at -80 ˚C) in a 1.5 ml eppendorf and removing excess ND96. 10 μl of homogenization buffer (100 mM NaCl, 50 mM Tris pH = 7.9, 0.6% SDS (w/v), 35 mM *n*-dodecyl β-D-maltoside (DDM) (Anatrace), and 1 protease inhibitor tablet) was added to the oocytes and oocytes were lysed manually with a pipette tip. The solution was sonnicated for 10 min and centrifuged for 30 min to

remove insoluble debris. The supernatant was transferred to a new eppendorf and 10 μl of 2X loading buffer was added. Samples were either stored at -80 ˚C or run on a gel.

Manual removal of membranes was performed as follows: oocytes were placed in hypotonic solution (5 mM NaCl, 5 mM HEPES pH = 7.5, 0.07% SDS (w/v)) and incubated for 10 min or until translucent oocyte membrane can be seen. The membrane was manually removed using forceps and placed in a 1.5 ml eppendorf kept on ice. 20 oocyte membranes were collected and then centrifuged for 10 min at 4 ˚C. The supernatant was removed and saved for Western blotting. 10 μl of smashing buffer (100 mM NaPhosphate pH = 7.8, 0.5% (w/v) DDM, and 1 protease inhibitor tablet) was added to the membranes. The membranes were sonnicated for 10 min and centrifuged for 10 min at 4 ˚C. The supernatant was removed from the insoluble fraction. 10 μl of 2X loading buffer was added to 10 μl of sample. Samples were either stored at -80 ˚C or run on a gel.

6.4.9 Western Blotting of Proteins Expressed in *Xenopus* Oocytes

Western blotting was performed as previously described (51). Briefly 20 μl of samples were loaded on a 4–15% linear gradient, polyacrylamide-ready gel Tris-HCl (Bio-Rad) or 15% polyacrylamide–ready gel Tris-HCl (Bio-Rad) and run at 150 V for 1.25 h. Protein was transferred to nitrocellulose (Bio-Rad) at 30 V for 30 min and 100 V for 1.5 h. Nitrocellulose was blocked overnight using BSA (for biocytin detection) or non-fat dairy milk (NFDM) (for subunit stoichiometry determination) in 1X PBS / 0.1% Tween. 12.5 μl of 1˚ Ab anti-HA from mouse and 5 μl of Streptavidn-AlexaFluor680 in 15 ml BSA / 1X PBS / 0.1% Tween was for 1 h, washed 4X with 30 ml 1X PBS / 0.1% Tween for 5 min each, placed in 3 μl 2˚ 800CW goat anti-mouse IgG in 15 mL BSA / 1X

PBS / 0.1% Tween was for 1 h, and washed 4X with 30 ml 1X PBS / 0.1% Tween for 5 min each. For subunit stoichiometry determination, the same procedure was used but NFDM replaced BSA and Streptavidin-680 was not used. Nitrocellulose was visualized using two-color infrared dye detection on the Odyssey (Li-Cor, Lincoln, NE) (Hsieh-Wilson lab). Densiometric analysis was performed using the Li-Cor Odyssey software package.

6.5 References

1. Prescher, J.A., and Bertozzi, C.R. (2005) Chemistry in living systems. *Nat. Chem. Biol.*, **1**, 13–21.

2. Griffin, B.A., Adams, S.R., and Tsien, R.Y. (1998) Specific covalent labeling of recombinant protein molecules inside live cells. *Science*, **281**, 269–272.

3. Adams, S.R., Campbell, R.E., Gross, L.A., Martin, B.R., Walkup, G.K., Yao, Y., Llopis, J., and Tsien, R.Y. (2002) New biarsenical ligands and tetracysteine motifs for protein labeling *in vitro* and *in vivo*: Synthesis and biological applications. *J. Am. Chem. Soc.*, **124**, 6063–6076.

4. Chen, I., Howarth, M., Lin, W., and Ting, A.Y. (2005) Site-specific labeling of cell surface proteins with biophysical probes using biotin ligase. *Nat. Methods*, **2**, 99–104.

5. Howarth, M., Takao, K., Hayashi, Y., and Ting, A.Y. (2005) Targeting quantum dots to surface proteins in living cells with biotin ligase. *Proc. Natl. Acad. Sci. USA*, **102**, 7583–7588.

6. Khidekel, N., Ficarro, S.B., Peters, E.C., and Hsieh-Wilson, L.C. (2004) Exploring the O-GlcNAc proteome: Direct identification of O-GlcNAc-modified proteins from the brain. *Proc. Natl. Acad. Sci. USA*, **101**, 13132–13137.

7. Laughlin, S.T., and Bertozzi, C.R. (2007) Metabolic labeling of glycans with azido sugars and subsequent glycan-profiling and visualization via Staudinger ligation. *Nat. Protoc.*, **2**, 2930–2944.

8. Chang, P.V., Prescher, J.A., Hangauer, M.J., and Bertozzi, C.R. (2007) Imaging cell surface glycans with bioorthogonal chemical reporters. *J. Am. Chem. Soc.*, **129**, 8400–8401.

9. Baskin, J.M., Prescher, J.A., Laughlin, S.T., Agard, N.J., Chang, P.V., Miller, I.A., Lo, A., Codelli, J.A., and Bertozzi, C.R. (2007) Copper-free click chemistry for dynamic *in vivo* imaging. *Proc. Natl. Acad. Sci. USA*, **104**, 16793–16797.

10. Yarema, K.J., Mahal, L.K., Bruehl, R.E., Rodriguez, E.C., and Bertozzi, C.R. (1998) Metabolic delivery of ketone groups to sialic acid residues. Application to cell surface glycoform engineering. *J. Biol. Chem.*, **273**, 31168–31179.

11. Saxon, E., and Bertozzi, C.R. (2000) Cell surface engineering by a modified Staudinger reaction. *Science*, **287**, 2007–2010.

12. Laughlin, S.T., Baskin, J.M., Amacher, S.L., and Bertozzi, C.R. (2008) *In vivo* imaging of membrane-associated glycans in developing zebrafish. *Science*, **320**, 664–667.

13. Datta, D., Wang, P., Carrico, I.S., Mayo, S.L., and Tirrell, D.A. (2002) A designed phenylalanyl-tRNA synthetase variant allows efficient *in vivo*

incorporation of aryl ketone functionality into proteins. *J. Am. Chem. Soc.*, **124**, 5652–5653.

14. Kiick, K.L., Saxon, E., Tirrell, D.A., and Bertozzi, C.R. (2002) Incorporation of azides into recombinant proteins for chemoselective modification by the Staudinger ligation. *Proc. Natl. Acad. Sci. USA*, **99**, 19–24.

15. Link, A.J., and Tirrell, D.A. (2003) Cell surface labeling of *Escherichia coli* via copper(I)-catalyzed [3+2] cycloaddition. *J. Am. Chem. Soc.*, **125**, 11164–11165.

16. Beatty, K.E., Xie, F., Wang, Q., and Tirrell, D.A. (2005) Selective dye-labeling of newly synthesized proteins in bacterial cells. *J. Am. Chem. Soc.*, **127**, 14150–14151.

17. Dieterich, D.C., Link, A.J., Graumann, J., Tirrell, D.A., and Schuman, E.M. (2006) Selective identification of newly synthesized proteins in mammalian cells using bioorthogonal noncanonical amino acid tagging (BONCAT). *Proc. Natl. Acad. Sci. USA*, **103**, 9482–9487.

18. Chin, J.W., Santoro, S.W., Martin, A.B., King, D.S., Wang, L., and Schultz, P.G. (2002) Addition of *p*-azido-L-phenylalanine to the genetic code of *Escherichia coli*. *J. Am. Chem. Soc.*, **124**, 9026–9027.

19. Wang, L., Zhang, Z., Brock, A., and Schultz, P.G. (2003) Addition of the keto functional group to the genetic code of *Escherichia coli*. *Proc. Natl. Acad. Sci. USA*, **100**, 56–61.

20. Zhang, Z., Smith, B.A., Wang, L., Brock, A., Cho, C., and Schultz, P.G. (2003) A new strategy for the site-specific modification of proteins *in vivo*. *Biochemistry*, **42**, 6735–6746.

21. Deiters, A., and Schultz, P.G. (2005) *In vivo* incorporation of an alkyne into proteins in *Escherichia coli*. *Bioorg. Med. Chem. Lett.*, **15**, 1521–1524.

22. Zeng, H., Xie, J., and Schultz, P.G. (2006) Genetic introduction of a diketone-containing amino acid into proteins. *Bioorg. Med. Chem. Lett.*, **16**, 5356–5359.

23. Meddows, E., Le Bourdelles, B., Grimwood, S., Wafford, K., Sandhu, S., Whiting, P., and McIlhinney, R.A. (2001) Identification of molecular determinants that are important in the assembly of N-methyl-D-aspartate receptors. *J. Biol. Chem.*, **276**, 18795–18803.

24. Atlason, P.T., Garside, M.L., Meddows, E., Whiting, P., and McIlhinney, R.A. (2007) N-Methyl-D-aspartate (NMDA) receptor subunit NR1 forms the substrate for oligomeric assembly of the NMDA receptor. *J. Biol. Chem.*, **282**, 25299–25307.

25. Keller, S.H., and Taylor, P. (1999) Determinants responsible for assembly of the nicotinic acetylcholine receptor. *J. Gen. Physiol.*, **113**, 171–176.

26. Ben-Ami, H.C., Yassin, L., Farah, H., Michaeli, A., Eshel, M., and Treinin, M. (2005) RIC-3 affects properties and quantity of nicotinic acetylcholine receptors via a mechanism that does not require the coiled-coil domains. *J. Biol. Chem.*, **280**, 28053–28060.

27. Saedi, M.S., Conroy, W.G., and Lindstrom, J. (1991) Assembly of *Torpedo* acetylcholine receptors in *Xenopus* oocytes. *J. Cell Biol.*, **112**, 1007–1015.

28. Wanamaker, C.P., Christianson, J.C., and Green, W.N. (2003) Regulation of nicotinic acetylcholine receptor assembly. *Ann. N.Y. Acad. Sci.*, **998**, 66–80.

29. Green, W.N. (1999) Ion channel assembly: Creating structures that function. *J. Gen. Physiol.*, **113**, 163–170.

30. Le Novere, N., Corringer, P.J., and Changeux, J.P. (2002) The diversity of subunit composition in nAChRs: Evolutionary origins, physiologic and pharmacologic consequences. *J. Neurobiol.*, **53**, 447–456.

31. Cooper, E., Couturier, S., and Ballivet, M. (1991) Pentameric structure and subunit stoichiometry of a neuronal nicotinic acetylcholine receptor. *Nature*, **350**, 235–238.

32. MacKinnon, R., Aldrich, R.W., and Lee, A.W. (1993) Functional stoichiometry of Shaker potassium channel inactivation. *Science*, **262**, 757–759.

33. Liman, E.R., Tytgat, J., and Hess, P. (1992) Subunit stoichiometry of a mammalian K^+ channel determined by construction of multimeric cDNAs. *Neuron*, **9**, 861–871.

34. He, Y., Ruiz, M., and Karpen, J.W. (2000) Constraining the subunit order of rod cyclic nucleotide-gated channels reveals a diagonal arrangement of like subunits. *Proc. Natl. Acad. Sci. USA*, **97**, 895–900.

35. Zheng, J., Trudeau, M.C., and Zagotta, W.N. (2002) Rod cyclic nucleotide-gated channels have a stoichiometry of three CNGA1 subunits and one CNGB1 subunit. *Neuron*, **36**, 891–896.

36. Zhong, H., Molday, L.L., Molday, R.S., and Yau, K.W. (2002) The heteromeric cyclic nucleotide-gated channel adopts a 3A:1B stoichiometry. *Nature*, **420**, 193–198.

37. Ulbrich, M.H., and Isacoff, E.Y. (2007) Subunit counting in membrane-bound proteins. *Nat. Methods*, **4**, 319–321.

38. Christianson, J.C., and Green, W.N. (2004) Regulation of nicotinic receptor expression by the ubiquitin-proteasome system. *EMBO J.*, **23**, 4156–4165.

39. Gallivan, J.P., Lester, H.A., and Dougherty, D.A. (1997) Site-specific incorporation of biotinylated amino acids to identify surface-exposed residues in integral membrane proteins. *Chem. Biol.*, **4**, 739–749.

40. Tzartos, S.J., Cung, M.T., Demange, P., Loutrari, H., Mamalaki, A., Marraud, M., Papadouli, I., Sakarellos, C., and Tsikaris, V. (1991) The main immunogenic region (MIR) of the nicotinic acetylcholine receptor and the anti-MIR antibodies. *Mol. Neurobiol.*, **5**, 1–29.

41. Mamalaki, A., and Tzartos, S.J. (1994) Nicotinic acetylcholine receptor: Structure, function and main immunogenic region. *Adv. Neuroimmunol.*, **4**, 339–354.

42. Miyazawa, A., Fujiyoshi, Y., and Unwin, N. (2003) Structure and gating mechanism of the acetylcholine receptor pore. *Nature*, **423**, 949–955.

43. Dahan, D.S., Dibas, M.I., Petersson, E.J., Auyeung, V.C., Chanda, B., Bezanilla, F., Dougherty, D.A., and Lester, H.A. (2004) A fluorophore attached to nicotinic acetylcholine receptor beta M2 detects productive binding of agonist to the alpha delta site. *Proc. Natl. Acad. Sci. USA*, **101**, 10195–10200.

44. Pantoja, R., Rodriguez, E.A., Dibas, M.I., Dougherty, D.A., and Lester, H.A. (2008) Single-molecule imaging of a fluorescent unnatural amino acid incorporated into functional nicotinic acetylcholine receptors. *Submitted*.

45. Saks, M.E., Sampson, J.R., Nowak, M.W., Kearney, P.C., Du, F.Y., Abelson, J.N., Lester, H.A., and Dougherty, D.A. (1996) An engineered *Tetrahymena* $tRNA^{Gln}$ for *in vivo* incorporation of unnatural amino acids into proteins by nonsense suppression. *J. Biol. Chem.*, **271**, 23169–23175.

46. Beene, D.L., Dougherty, D.A., and Lester, H.A. (2003) Unnatural amino acid mutagenesis in mapping ion channel function. *Curr. Opin. Neurobiol.*, **13**, 264–270.

47. Dougherty, D.A. (2000) Unnatural amino acids as probes of protein structure and function. *Curr. Opin. Biotechnol.*, **4**, 645–652.

48. Rodriguez, E.A., Lester, H.A., and Dougherty, D.A. (2007) Improved amber and opal suppressor tRNAs for incorporation of unnatural amino acids *in vivo*. Part 1: Minimizing misacylation. *RNA*, **13**, 1703–1714.

49. Rodriguez, E.A., Lester, H.A., and Dougherty, D.A. (2006) *In vivo* incorporation of multiple unnatural amino acids through nonsense and frameshift suppression. *Proc. Natl. Acad. Sci. USA*, **103**, 8650–8655.

50. Rodriguez, E.A., Lester, H.A., and Dougherty, D.A. (2007) Improved amber and opal suppressor tRNAs for incorporation of unnatural amino acids *in vivo*. Part 2: Evaluating suppression efficiency. *RNA*, **13**, 1715–1722.

51. England, P.M., Zhang, Y.N., Dougherty, D.A., and Lester, H.A. (1999) Backbone mutations in transmembrane domains of a ligand-gated ion channel: Implications for the mechanism of gating. *Cell*, **96**, 89–98.

52. England, P.M., Lester, H.A., and Dougherty, D.A. (1999) Mapping disulfide connectivity using backbone ester hydrolysis. *Biochemistry*, **38**, 14409–14415.

53. Watanabe, T., Muranaka, N., Iijima, I., and Hohsaka, T. (2007) Position-specific incorporation of biotinylated non-natural amino acids into a protein in a cell-free translation system. *Biochem. Biophys. Res. Commun.*, **361**, 794–799.

54. Changeux, J.P., Kasai, M., and Lee, C.Y. (1970) Use of a snake venom toxin to characterize the cholinergic receptor protein. *Proc. Natl. Acad. Sci. USA*, **67**, 1241–1247.

55. Green, N.M. (1990) Avidin and streptavidin. *Methods Enzymol.*, **184**, 51–67.

56. Drenan, R.M., Nashmi, R., Imoukhuede, P., Just, H., McKinney, S., and Lester, H.A. (2008) Subcellular trafficking, pentameric assembly, and subunit stoichiometry of neuronal nicotinic acetylcholine receptors containing fluorescently labeled alpha6 and beta3 subunits. *Mol. Pharmacol.*, **73**, 27–41.

57. Jansen, M., Bali, M., and Akabas, M.H. (2008) Modular design of Cys-loop ligand-gated ion channels: Functional 5-HT3 and GABA rho1 receptors lacking the large cytoplasmic M3M4 loop. *J. Gen. Physiol.*, **131**, 137–146.

58. Brandt, G.S. (2003) *Ph. D. Thesis*, California Institute of Technology, Pasadena, CA.

59. Shafer, A.M., Kalai, T., Bin Liu, S.Q., Hideg, K., and Voss, J.C. (2004) Site-specific insertion of spin-labeled L-amino acids in *Xenopus* oocytes. *Biochemistry*, **43**, 8470–8482.

60. Tokmakov, A.A., Matsumoto, E., Shirouzu, M., and Yokoyama, S. (2006) Coupled cytoplasmic transcription-and-translation—a method of choice for heterologous gene expression in *Xenopus* oocytes. *J. Biotechnol.*, **122**, 5–15.

61. Harel, M., Kasher, R., Nicolas, A., Guss, J.M., Balass, M., Fridkin, M., Smit, A.B., Brejc, K., Sixma, T.K., Katchalski-Katzir, E. *et al.* (2001) The binding site of acetylcholine receptor as visualized in the X-Ray structure of a complex between alpha-bungarotoxin and a mimotope peptide. *Neuron*, **32**, 265–275.

62. West, A.P., Jr., Bjorkman, P.J., Dougherty, D.A., and Lester, H.A. (1997) Expression and circular dichroism studies of the extracellular domain of the alpha subunit of the nicotinic acetylcholine receptor. *J. Biol. Chem.*, **272**, 25468–25473.

63. Blount, P., and Merlie, J.P. (1988) Native folding of an acetylcholine receptor alpha subunit expressed in the absence of other receptor subunits. *J. Biol. Chem.*, **263**, 1072–1080.

64. Claudio, T., Paulson, H.L., Green, W.N., Ross, A.F., Hartman, D.S., and Hayden, D. (1989) Fibroblasts transfected with Torpedo acetylcholine receptor beta-, gamma-, and delta-subunit cDNAs express functional receptors when infected with a retroviral alpha recombinant. *J. Cell Biol.*, **108**, 2277–2290.

65. Robertson, S.A., Noren, C.J., Anthony-Cahill, S.J., Griffith, M.C., and Schultz, P.G. (1989) The use of 5'-phospho-2 deoxyribocytidylylriboadenosine as a facile route to chemical aminoacylation of tRNA. *Nucleic Acids Res.*, **17**, 9649–9660.

66. Kearney, P.C., Nowak, M.W., Zhong, W., Silverman, S.K., Lester, H.A., and Dougherty, D.A. (1996) Dose-response relations for unnatural amino acids at the agonist binding site of the nicotinic acetylcholine receptor: Tests with novel side chains and with several agonists. *Mol. Pharmacol.*, **50**, 1401–1412.

67. Zhong, W., Gallivan, J.P., Zhang, Y., Li, L., Lester, H.A., and Dougherty, D.A. (1998) From ab initio quantum mechanics to molecular neurobiology: A cation-π

binding site in the nicotinic receptor. *Proc. Natl. Acad. Sci. USA*, **95**, 12088–12093.

68. Nowak, M.W., Gallivan, J.P., Silverman, S.K., Labarca, C.G., Dougherty, D.A., and Lester, H.A. (1998) *In vivo* incorporation of unnatural amino acids into ion channels in *Xenopus* oocyte expression system. *Meth. Enzymol.*, **293**, 504–529.

69. Petersson, E.J., Shahgholi, M., Lester, H.A., and Dougherty, D.A. (2002) MALDI-TOF mass spectrometry methods for evaluation of *in vitro* aminoacyl tRNA production. *RNA*, **8**, 542–547.

70. Quick, M.W., and Lester, H.A. (1994) Methods for expression of excitability proteins in *Xenopus* oocytes. In Narahashi, T. (ed.), *Ion Channels of Excitable Cells*. Academic Press, San Diego, CA, Vol. 19, pp. 261–279.